Research Article

Microstructural and Mechanical Behaviors of Friction Stir Welded Dissimilar AA6082-AA7075 Joints

M. Vetrivel Sezhian,[1] K. Giridharan,[1] D. Peter Pushpanathan,[1] G. Chakravarthi,[1] B. Stalin ⓘ,[2] Alagar Karthick ⓘ,[3] P. Manoj Kumar,[4] and Murugesan Bharani ⓘ[5]

[1]*Department of Mechanical Engineering, Easwari Engineering College, Chennai 600089, Tamilnadu, India*
[2]*Department of Mechanical Engineering, Anna University, Regional Campus Madurai, Madurai 625019, Tamilnadu, India*
[3]*Department of Electrical and Electronics Engineering, KPR Institute of Engineering and Technology, Coimbatore 641407, Tamilnadu, India*
[4]*Department of Mechanical Engineering, KPR Institute of Engineering and Technology, Coimbatore 641407, Tamilnadu, India*
[5]*School of Textile Leather and Fashion Technology, Kombolcha 208, Kombolcha Institute of Technology, Wollo University, South Wollo, Ethiopia*

Correspondence should be addressed to Murugesan Bharani; bharani.murugesan@kiot.edu.et

In this research, microstructural events and mechanical behaviors in dissimilar friction stir welding (FSW) of aluminium (Al) alloy AA6082-AA7075 joints have been evaluated to apply aerospace, defense, and military sectors. FSW parametric effects have a more significant impact on the mechanical performances and microstructure of produced joints. FSW tool rotational speed, welding speed, and tool plunge speed were chosen to make the weld joints. The rotational tool speeds of 1600 rpm and 2300 rpm, welding speeds of 40 mm/min and 60 mm/min, and tool plunge speeds of 20 mm/min and 30 mm/min were set as the upper and lower limits. A constant axial force of 5 kN was maintained throughout the joint fabrication process. A taper pin-profiled tool was utilized to produce the butt welded joints. Mechanical properties of microhardness, tensile strength, yield strength, elongation, and bending strength of the joints were analyzed. The response of the stir zone microstructure to processing parameters was evaluated using optical microscopy (OM) and fractographic analysis of a tensile specimen shown by scanning electron microscope (SEM). The weld joints produced at 2300 rpm, tool traveling rate of 40 mm/min, and tool plunge speed of 30 mm/min showed the greatest tensile strength of the 191 MPa hardness of 145 Hv at the weld center and also the maximum bending strength of 114.23 N/mm^2 was achieved. The lowest bending strength of 25.38 N/mm^2 was obtained at 1600 rpm with 60 mm/min due to inappropriate mixing of the base metals and poor joint quality. Furthermore, this study revealed that a higher tool plunge speed facilitates the formation of equiaxed grains in the thermomechanically affected zone (TMAZ) on the advancing side (AS). Additionally, the increment in tool rotational speed significantly improved the tensile strength, weld joint quality, and joint efficiency.

1. Introduction

Aluminum alloys are lightweight and have more applications in the industrial sector. By conventional fusion welding techniques, aluminum alloys are tough to weld, and the joint quality is also unsuitable due to welding defects like distortion, cracks, and porosity [1]. FSW has recently been selected as a reliable method for retaining the alloy's properties when the joining takes place in the solid state. This technique is performed for joining different material combinations, such as aluminum, copper, magnesium, brass, and other material types. FSW tool plays a very important role in the material joining processes [2]. The usage of aluminum alloys is rapidly increasing due to their castability, lightweight structures needing a higher strength ratio, and extraordinary corrosion resistance. The various

FSW tool pin profiles are used to make weld joints between two materials. It has been reported that the tapered pin-profiled tool produced sound (defect-free) weld joints when compared to other pin profiles [3]. Aluminum alloys find various applications in the wing structure, fuel tanks, railway tanks, vehicle bridges, high-speed ships, aerospace, engine chassis, automotive industries, and military applications due to their lightweight and greater strength and weight ratio [1–4]. FSW is a solid-state material joining technique developed by The Welding Institute (TWI) in 1991.

To fabricate weld joints between two metals, a nonconsumable rotating tool was used, which eliminated the need for additional filler materials. This process does not release toxic or nontoxic fumes during material joining and develops welds free from solidification effects. This technique was recently developed and is highly important for the material joining of similar and dissimilar materials [5, 6]. The FSW process produces an attractive solid- phase bond in the material joining process without melting and recasting the parent materials [7]. FSW weld joint consists of a heat-affected zone (HAZ) and TMAZ. It has produced defect-free weld joints with more excellent mechanical properties and minimum welding defects [8]. The rotational tool speed was the major influential factor in producing sound weld joints. This method has more significant potential for joining aluminum alloys since it can reduce welding defects like porosity, welding cracks, and distortions, commonly encountered in other fusion welding techniques [7–9].

The various effects of the FSW parameters have been discussed, like welding speed, tool revolving speed, axial load, and tool pin profile. However, the effect of the tool plunge speed has not been reported to date. It was identified that the grain size of the particle and hardness value of the nugget zone varies, purely depending on the welding tool rotational speed and tool traveling speed [10]. The FSW welding parameters play an essential function in the quality of the weld joints while fabricating them. The mechanical and microstructural properties were investigated in a pair of AA2024 and AA7075 aluminum alloys. The obtained hardness value of the weld joints is decreased when moved away from their center [11]. Better hardness values were obtained in the nugget zone more than other zones affected by the welding process [12]. The FSW tool features like shoulder diameter and taper pin profile are instrumental in producing adequate weld surface quality and better mechanical behaviors of sound weld joints [13]. The weld joints' properties and features were investigated. A large amount of frictional heat is produced in the obtained weld joints based on the FSW process parameters like revolving tool speed (rpm), tool traveling speed (mm/min), pin plunge depth (mm), and axial force (kN) [14]. The effects of the FSW parameters and tool pin profile on the tensile strength, microstructural analysis, hardness, and fatigue behavior of weld joints were experimentally investigated. The welding speed and tool traveling speed were found to help in deciding the joint strength [15].

Many researchers have successfully investigated and reported the microstructural characteristics and mechanical behaviors of dissimilar aluminum alloys processed by FSW.

However, the literature available on the bending characteristics of dissimilar aluminum butt joints between the AA6xxx and AA7xxx series is limited. Therefore, this research presents the mechanical properties, microstructural analysis, and bending characteristics of AA6082-AA7075 dissimilar weldments fabricated with various FSW parameters.

2. Materials and Methodology

2.1. Materials. AA6082 and AA7075 aluminum alloys were taken as the parent materials in this investigation with 2000 mm × 1500 mm × 5 mm. The base materials were prepared to the required dimensions utilizing a milling machine. The base materials for both AA6082-AA7075 aluminum alloys were resized to the required length (100 mm) and width (50 mm) utilizing an automatic material cutting machine (power hacksaw), and a milling machine was utilized to remove the sharp edges of the base materials. Besides, the maximum amount of manganese present in the parent material controls the grain structure. These features could be helpful to obtain good results and quality of the weld joints. Tables 1–3 represent the mechanical properties, physical properties, and chemical composition of the base materials.

A detailed investigation of previous literature according to Sevvel et al. [18] reports that tool geometry of FSW is the most significant feature of the material joining process. Tool pin geometry plays an essential role in the material flow and turn and governs the transverse rate at which FSW can be calculated. M35 grade tool steel material is selected to fabricate the friction stir welding tool due to its high strength, excellent wear resistance, and low material cost. The taper cylindrical pin-profiled tool was utilized to make the weld joints. A shoulder diameter of 12 mm, pin length of 4.85 mm, and pin with 7 mm to 4 mm diameter were maintained while fabricating the FSW tool. This tool material provides more resistance to softening, especially while working at high temperatures likes 550–600°C at maximum operating tool speeds. Figure 1(a) and 1(b) show a schematic view and dimensions of the fabricated FSW tool.

2.2. FSW Parameters and Experimental Work. A conventional vertical milling machine FSW setup was used to make the weld joints. The FSW equipment is equipped with a 5 kW motor power pack. The length of the bed is 810 mm and the width 40 mm; this is housed at SA Engineering College, Chennai. The photographic view of the FSW arrangement and joining process is shown in Figure 2(a) and 2(b). The base material AA6082-AA7075 dissimilar aluminum alloys were used to fabricate the weld joints. Before starting the FSW process, the base material surface was thoroughly cleaned of the rust, burs, dirt, and oxide layers. The thickness of both materials was maintained at 5 mm. Then, the alloy plates were securely clamped with the help of a manual top clamp set up on the machine bed surface in a butt joint configuration so that it does not disturb the welding process.

TABLE 1: Mechanical properties of base material AA6082-AA7075 aluminum alloy.

Base material	AA6082	AA7075
Elastic modulus (N/mm^2)	7.1×10^3	7.2×10^3
Ultimate tensile strength (MPa)	279	502
Yield strength (MPa)	244	398
Elongation percentage in 25 mm GL%	18.5	17.1

TABLE 2: Physical properties of base material alloys [16, 17].

Material	Thermal conductivity (W/m·k)	Electrical conductivity (% IACs)	Density (kg/m^3)	Thermal expansion (k)
AA6082	182	29	2710	23×10^{-6}
AA7075	134	33	2810	23.5×10^{-6}

TABLE 3: Chemical composition of AA6082 and AA7075 Al alloys in wt%.

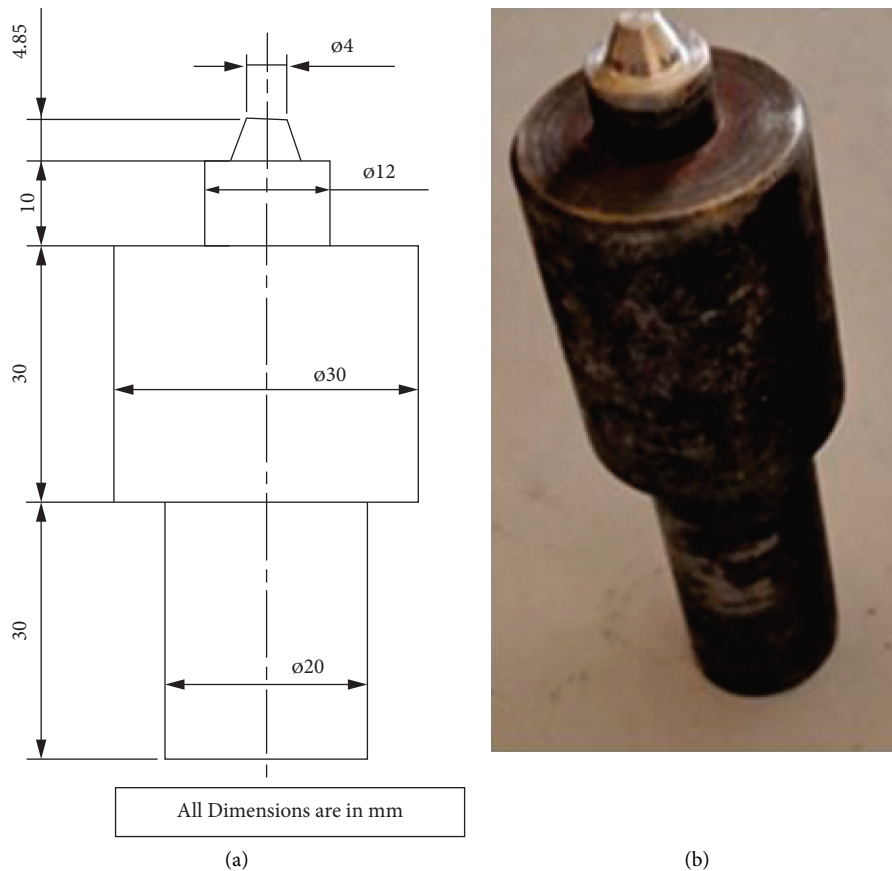| Elements	Si	Fe	Cu	Mn	Mg	Cr	Zn	Ti	Al
AA6082	0.84	0.31	0.086	0.587	1.123	0.03	0.016	0.02	Balance
AA7075	0.056	0.089	1.564	0.159	0.239	0.190	0.531	0.037	Balance

(a)   (b)

FIGURE 1: Geometry and photographic view of the FSW tool.

Al alloy AA6082 was placed on the AS, and AA7075 alloy was placed on the retreating side (RS). The taper pin-profiled stir tool was fixed on the machine spindle. The material joining process took place along the rolling direction of base materials. The welding process was conducted at different spindle speeds of 1600 rpm and 2300 rpm, tool traveling speeds of 40 mm/min and 60 mm/min, and tool plunge speeds of 20 mm/min and 30 mm/min, maintaining a
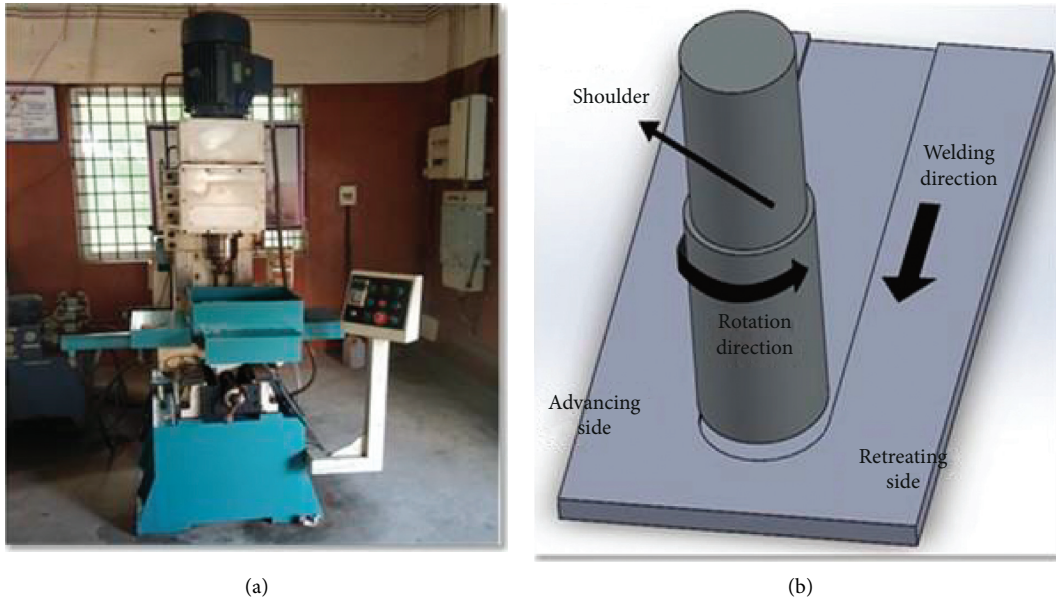
(a)   (b)

FIGURE 2: Photographic view of FSW arrangement and joining process.

constant axial load of 5 kN and tool tilt angle of 0°. The tool plunge depth of 0.25 mm and plunge speed of 30 mm/min and 40 mm/min were maintained throughout the welding process.

The welding process parameters utilized in this work are listed in Table 4, and the process parameter combinations formed as per Taguchi L8 orthogonal array are presented in Table 5. Initially, the FSW spindle rotation is started with the required speed without touching the base material surfaces. Then, the designed FSW stirred pin is inserted to a predetermined plunge depth between the two base materials to be welded at the desired plunge speeds. The tool is revolved continuously to maintain the dwell time of 1 min without moving the stirred pin; meanwhile, the frictional heat produced softens the base materials. After the dwell time, the FSW tool moves along the weld direction to the base materials, producing the weld joints.

The tool is retracted after the welding process does it. The photographic view of the joints before and after welding is depicted in Figures 3(a)–3(c).

3. Testing of the Weld Samples

3.1. Tensile Test. The tensile test specimens were developed as per the ASTM-E8-04 standard. The tensile specimen dimensions are depicted in Figure 4. The sample was cut to the proper dimensions perpendicular to the weld direction by using wire cut EDM. The prepared tensile specimen was inspected after machining. The universal testing machine (UTM) was utilized to assess the tensile test on the weld samples. The weldments were tested as per the standard. The % of elongation, yield stress, and tensile strength of the welded joints were obtained. The tensile strengths of the weldments are presented in Table 6.

TABLE 4: Factors selected and their levels.

Factors	Levels	
	High	Low
Welding speed (V) (mm/min)	60	40
Tool rotational speed (N) (rpm)	2300	1600
Plunge speed (P) (mm/min)	30	20

TABLE 5: Factors set based on L8 orthogonal array.

S. no.	Experiment number	Tool rotational speed (rpm)	Tool traveling speed (mm/min)	Plunge speed (mm/min)
1	FSW-L1	1600	40	20
2	FSW-L2	1600	40	30
3	FSW-L3	1600	60	20
4	FSW-L4	1600	60	30
5	FSW-L5	2300	40	20
6	FSW-L6	2300	40	30
7	FSW-L7	2300	60	20
8	FSW-L8	2300	60	30

3.2. Hardness Test. A hardness test was conducted across the various FSW zones of the weld joints, utilizing the Vickers hardness testing machine. Hardness values are reported in Table 4. The weld specimens were fabricated and processed by the FSW technique. The size of the grains in the different welding zones plays an important role in evaluating the hardness of the weld joints. The small-sized grain particles give massive strength or the highest hardness values, due to which the grain boundaries avoid slip and dislocations [19]. It is identified that the grain sizes were reduced in the weld zone, which increases the hardness values simultaneously. In the present experimental work, defect-free weldments, due to excellent equiaxed grain particles, were found in the weld
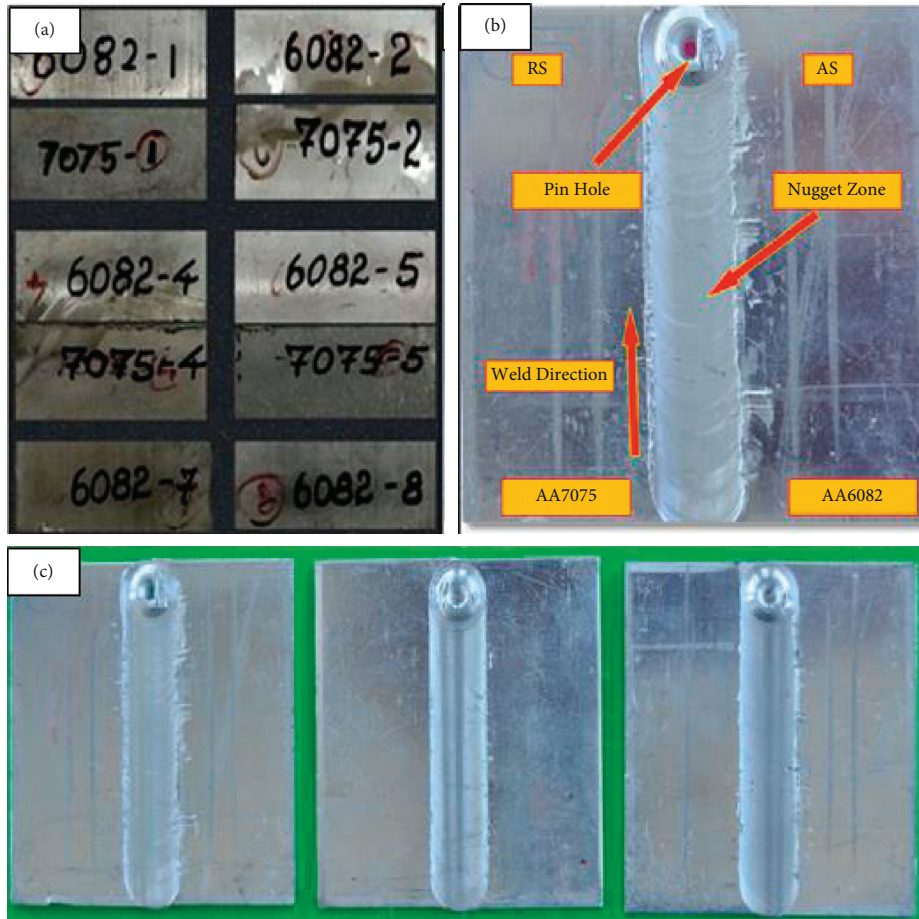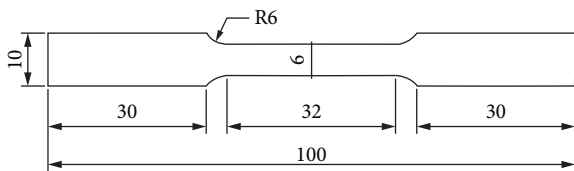
FIGURE 3: A photographic view of the joints before and after welding.

FIGURE 4: Tensile test sample dimensions (ASTM-E8-04).

nugget zone, compared to both parent materials. The maximum hardness values are recorded in the nugget zone nearly close to the base material hardness value due to the presence of refined equiaxed grains homogeneously distributed in the nugget zone. Mechanical behaviors of the weld specimens are given in Table 6. The effect of temperature on welded joints was studied, and it was shown that greater welding speeds and feeds resulted in higher temperatures. The weld bead softened and the microhardness decreased as the values of these parameters increased [20].

3.3. Bending Test. The bending strength of the base materials was successfully tested by the three-point method, and the characteristics are presented in Table 7. The bending test samples were developed following the ASTM-E290-08 standard. Figure 5(a) illustrates that a sample size of 100 mm × 12 mm × 5 mm was maintained for all the bending samples. The indenter corner radius is 10 mm. Figures 5(b) and 5(c) show the base alloys' photographic view. Figure 5(d) indicates weld samples used for the bend test. A bending test was successfully conducted to assess the weld samples' joint strength (bond strength).

TABLE 6: Mechanical behaviors of welded joints.

Sample no.	Hardness in Hv 100 gm	Ultimate tensile strength (MPa)	Yield strength (MPa)	% of elongation in 50 mm
1	127	143	132	22.5
2	102	125	121	12.04
3	121	154	112	18
4	115	131	108	23
5	135	189	121	22.05
6	145	191	132	23.5
7	105	144	127	14.05
8	116	162	98	19.8

TABLE 7: Bending strength of the base materials.

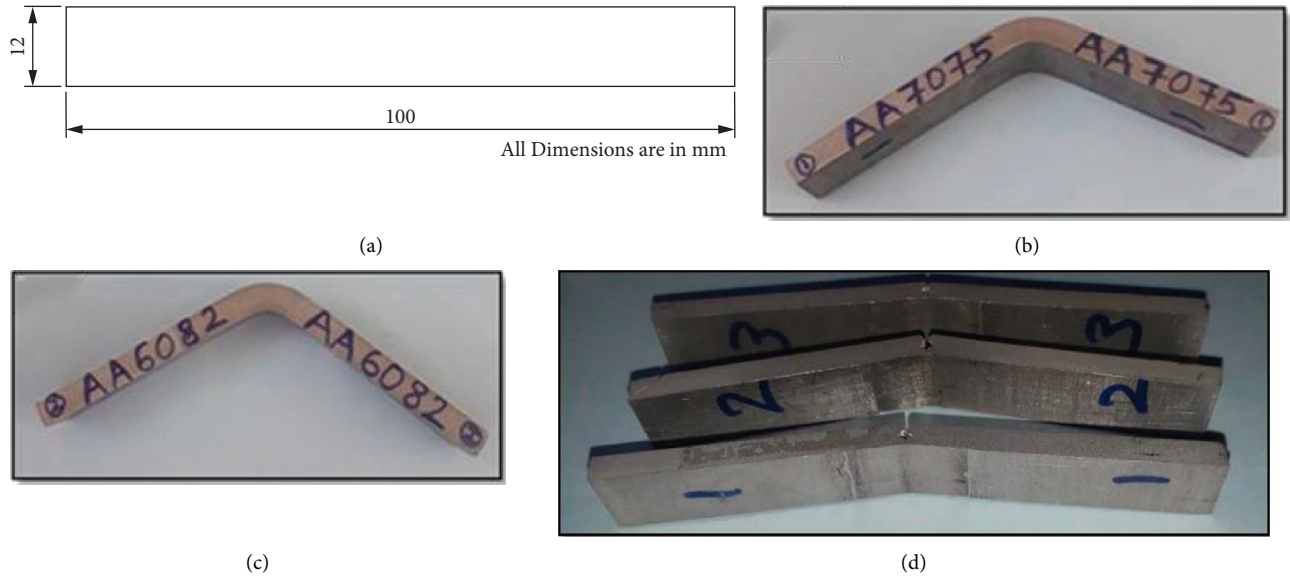| Parent material	Mandrel diameter (mm)	Angle of bend (degrees)	Ultimate/ breaking load (kN)	Displacement "F" max. (mm)	Maximum displacement (mm)	Bending strength (N/mm^2)	Remarks
AA6082	4T	180	0.505	11.2	18.5	116.53	No openings and no cracks observed
AA7075	4T	180	0.408	10.89	17.23	94.15	No openings and no cracks observed

(a)

(b)

(c)

(d)

FIGURE 5: (a) Top view of bend sample as per the ASTM standard. (b, c) Photographic view of base material bend samples. (d) Photographic view of bend samples after the experiment.

4. Results and Discussion

4.1. Appearance of Weld Joints. The schematic top view of the FSW samples is shown in Figure 3. The FSW process successfully processed the weld samples using a tool steel M35 grade FSW tool with a tapered pin profile. The physical appearance of the weld joints joined with 1600, 2300 rpm tool rotational speeds and 40, 60 mm/min welding speeds seems good without any defects. The pin plunging speed of 20, 30 mm/min was utilized in this process. Due to the FSW tool plunging into the interface of the weld joint, the surface of the weld region contained a slight concavity. As a result, a small number of weld flashes was produced in the weld region of the specimens.

4.2. Macro- and Microstructural Analysis. Following the joint fabricating process, samples were prepared for micro- and macroanalysis using standard metallographic methods. First, the etching process was performed using 50 mL H_3PO_4 and 1 gram of NaCl dissolved in 125 mL of ethanol to the weld zone for 60 seconds. Further, the same process was followed for 12 seconds using 4 grams of $KMnO_4$ and 1 gram

of sodium hydroxide (NaOH) dissolved in 120 mL of distilled water [21]. After that, each weld sample was observed with a high-resolution optical microscope. Figure 6(a) illustrates the microstructure of the parent material AA6082 aluminum alloy. It shows the size of the grain particle changing from 7 μm to 12 μm. Figure 6(b) illustrates the microstructure of the base material AA7075 aluminum alloy. It shows the size of the grain particle changing from 6 μm to 12 μm. The frictional heat increased at the weld region due to the increment in the rotational tool speed. Also, the increment in the welding speed produces the highest cooling rate [22].

The weld sample joined by the combination of the maximum tool rotational speed of 2300 rpm and minimum welding speed of 40 mm/min yielded the high tensile strength of 191 MPa, bending strength of 114.23 N/mm^2, and the highest hardness of 145 Hv, which are nearly 85% of the base metals. In the welding of Ti6Al4V plates, the tensile strength improved significantly. The primary contributing factor was found to be the formation of lamellar structures. During the operation, however, the hardness of the stir zone decreased due to grain coarsening and dynamic recrystallization [23]. The maximum FSW tool speed and lower
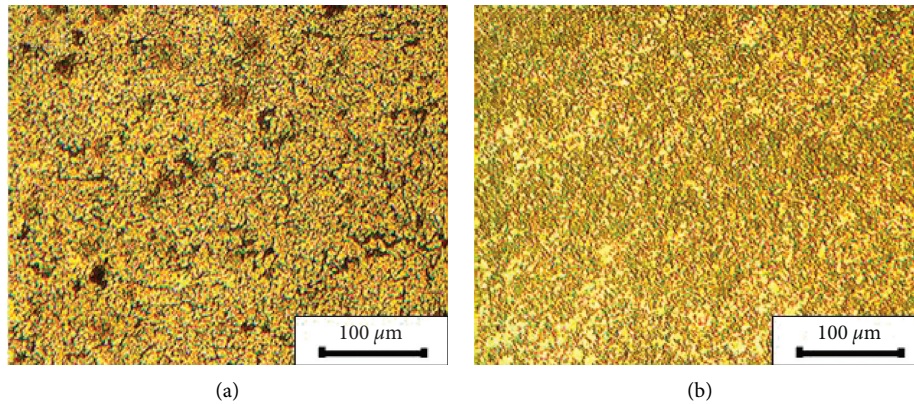
Figure 6: A photographic view of the microstructure of the AA6082-AA7075 alloys.

welding speed result in insufficient heat input during the welding process. The minimum welding rate provides a lesser cooling rate [24]. The highest tool speed and lower tool traveling (welding rate) give longer interaction time between the FSW tool pin and the weld samples, which leads to perfect material transportation and string starting from the AS to RS and from the RS to AS [25]. Therefore, fine grain with equiaxed particles evenly distributed (Figure 7(a)) in the nugget (weld region) zone led to producing defect-free weld joints (Table 8). Tunnel defects were found just above the bottom of the welded region in the examination of dissimilar welding of Al 5052 and 304 SS alloys. During the microstructural examination, the defects were found to be on the retreating side. Other defects, including voids and cracks, were found regardless of process parameter selection [26].

The weld sample produced by the maximum FSW tool rotation speed of 2300 rpm and higher welding rate of 60 mm/min exhibited average tensile strength (162 MPa), as shown in Figure 7(b). Due to increasing spindle speed and tool traveling rate, the cooling rate might be higher when compared to the other weld samples. The increasing welding speed and tool rotation speed reduce the interaction time of the weld samples and the tool, leading to inappropriate material mixing in the nugget zone and inadequate material consolidation. The weld sample joined by the minimum tool rotation speed of 1600 rpm and minimum welding speed of 40 mm/min exhibited lower tensile strength (125 MPa). Insufficient frictional heat was developed while using a lower tool rotating speed during the joint fabricating process. The cooling rate is too low for this parameter. The nugget zone reaction between materials purely depends on the lack of heat generation. Figure 7(c) shows low frictional heat produced during the joint making process (welding), leading to the tunnel defect, breaking, and distribution of particles in the nugget region, which provides inadequate material transport and inappropriate material string nugget region in the weld zone. The back-assisted FSW technique was used to examine the mechanical and microstructural characteristics of dissimilar NiTi-Ti6Al4V joints. It was revealed that defect joints can be obtained to increase the plastic fluidity of the welded metals. The mechanical characteristics of the joints were deteriorated by the coarse and brittle intermetallic compounds formed during the process [27]. Table 8 represents the volume defects that have been noticed in the nugget zone (weld region) with a minimum tensile strength of the weld joint.

The existence of approximately equal volumes of austenite and ferrite phases in the stir zone was reported in a study of dissimilar FSW of 304 ferritic and austenitic steels, which contributed to the creation of defect-free joints [28]. The weld joints fabricated with a higher tool rotational speed of 2300 rpm and minimum tool traveling speed of 40 mm/min exhibited the highest tensile and hardness values due to equal-sized fine grain particles distributed in the weld region. The high tensile and hardness values were obtained using a lower spindle speed and tool traveling speed. Hence, the tensile-tested samples were fractured on the RS [29]. The lower hardness value of the weldments was observed in HAZ. A microhardness study was conducted on dissimilar AA6061-T6 and AA5052-H32 welded joints revealed the presence of lower hardness on both sides of HAZ. Though the nugget zones exhibited higher hardness, they also showed the presence of some cracks due to higher welding speeds [30].

An advanced numerical model was developed and the experimental studies were carried out to validate the properties of underwater FSW dissimilar aluminium and steel joints. The maximum temperature was recorded on the steel side due to the higher melting point. The peak temperature increased with the heat input index defined in terms of the ratio of tool rotation speed and welding speed. Heat input index played a major role in the mixing and diffusion of aluminium into steel for the submerged underwater welding condition [31].

The influence of cooling media on the microstructure of dissimilar AA3003 aluminum and A441 AISI steel joints was investigated with CO_2, air, and water. CO_2 suppressed the grain growth due to recrystallization and reduced the thickness of the intermetallic compound layer at the joint. However, water proved to be the better cooling media as it produced joints with no notable segregations and better mechanical properties [32].

4.3. Bending Characteristics of the Weld Joints. Bending tests were conducted on all the weld joints by the three-point bend method to evaluate the flexural strength of the
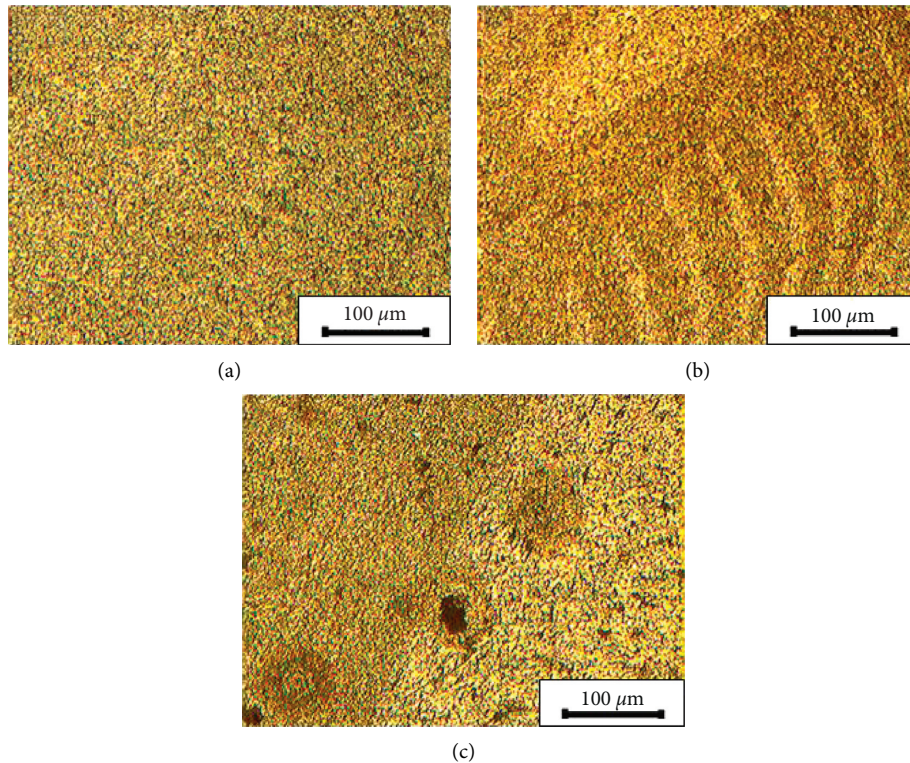
(a)

(b)

(c)

FIGURE 7: Photographic view of optical microstructures: (a) weld sample prepared with 2300 rpm and 40 mm/min, (b) weld sample prepared with 2300 rpm and 60 mm/min, and (c) weld sample fabricated with 1600 rpm and 40 mm/min.

weldments. The bent test sample was prepared following the ASTM-E290 standard to evaluate the material consolidation, ductility of the weldments, and bond strength. A size of $100 \times 12 \times 5$ mm dimensions was maintained to fabricate the bend test samples using EDM. Each weld sample subjected to the bend test is evaluated with a mandrel size of 4 T at 180°. The experimental observations of the bending samples like bending strength, maximum displacement, and breaking load are listed in Table 9. For all the FSW experimental work, rotational tool speed and welding speed significantly alter the bending strength by influencing the heat generated in the weld zones. In the center of the weld joint, the bending force was applied, and the test sample's back surface was observed. At the end of the bend test, no surface cracks were observed, indicating that the weld joint possessed good ductility. However, a few weld samples were identified with bottom side irregularities resulting in the poor bending strength of the joints.

The applied force and maximum displacement of the test samples were recorded precisely during the testing process. The bending strength of all the FSW AA6082-AA7075 different weld samples was lower than that of the parent materials. A minor crack was noticed at the back surface of the weld specimen joined at 1600 rpm due to poor mixing of materials caused by the lower axial force during the welding process. Another reason for attaining minor cracks was the lack of FSW tool pin penetration on the root site of the weld sample. After the bending test, the defects were identified in the root side for a few samples due to tunnel defects. Even

though the weld sample surface appeared friendly, tunnel defects were observed on the RS and the nugget zone of the weld. Figures 8(a)–8(d) show a graphical representation of the bending strength values for defect-free and defective weld samples. The plasticized material below the shoulder is insufficient during the material joining process due to improper frictional heat generation. This problem can be identified by increasing the welding speed and reducing the rotational tool speed [29].

4.4. Fractography of Tensile Test Specimen. Figure 9 indicates fracture morphology of FSW weld samples tested as per ASTM-E8-04 for tensile strength. The majority of the tensile test samples were fractured in their lower level of the hardness region. The weld specimens were fabricated at 2300 rpm at the welding speed of 40 mm/min fractured on the base material side. The weld samples fractured on the weld and HAZ zone were fabricated at 1600 rpm and the welding speed of 60 mm/min. The tensile strength of the weld samples is reduced by increasing the FSW tool rotation speed and at minimum welding speed. The high tensile strength of 191 MPa was obtained from a tool speed of 2300 rpm, tool travel rate of 40 mm/min, and tool plunge speed of 30 mm/min. The SEM images of the fractured weld samples depicted in Figure 10 were produced at the rotational tool speed of 2300 rpm. The fractographs of the welded samples revealed a ductile mode of fracture. SEM images of the fractured surfaces presented in Figures 10(a)–10(d)

TABLE 8: Macrostructures of weld joints cross sections.

Sample no.	Macrographs of the cross section of weld joints	Weld joint quality
6	 2 mm/10X Joint fabricated at 2300 rpm & 40 mm/min	Good (defect-free weldment)
5	 2 mm/10X Joint fabricated at 2300 rpm & 40 mm/min	Good (defect-free weldment)
1	 2 mm/10X Joint fabricated at 2300 rpm & 60 mm/min	Acceptable weld joint inadequate material mixing on the retreating side
8	 2 mm/10X Joint fabricated at 2300 rpm & 60 mm/min	Acceptable weld joint with tunnel defect on joint line at the bottom
3	 2 mm/10X Joint fabricated at 1600 rpm & 40 mm/min	Poor weld joint with tunnel defect on the retreating side
2	 2 mm/10X Joint fabricated at 1600 rpm & 40 mm/min	Poor weld joint with tunnel defect on the retreating side

exhibit dents and clefts. On the serrated surface of the fractured tensile samples, cleavage planes and fine dimples were apparent. The increment in the strength of the joints is attributed to grain refinement. The integrity of the dissimilar 2024 and 7075 aluminium alloys was assessed in terms of residual stress distribution. Residual stress profiles generated by the neutron diffraction method indicated that the transverse and the normal tensile stresses were present on the 7075 sides. However, the 2024 side exhibited compressive stresses [33].

TABLE 9: Bending test results for weld samples.

| Experiment number	Type of bending	Ultimate/ breaking load (kN)	Displacement "F" max. (mm)	Maximum displacement (mm)	Bending strength (N/mm^2)	Remarks
FSW-1	Face bend	0.315	8.5	12.14	72.69	No cracks and openings observed
FSW-2	Face bend	0.205	1.34	3.95	47.30	Minor cracks observed
FSW-3	Face bend	0.190	1.0	3.90	43.84	No cracks and openings observed
FSW-4	Face bend	0.195	1.10	3.40	25.38	Cracks and openings observed
FSW-5	Face bend	0.490	12.6	14.0	113.07	Obtained U-shaped bend. No cracks and openings observed
FSW-6	Face bend	0.495	10.3	15.2	114.23	Obtained U-shaped bend. No cracks and openings observed
FSW-7	Face bend	0.178	0.60	6.50	41.07	Cracks and openings observed on the root side
FSW-8	Face bend	0.174	0.50	6.20	40.15	Minor crack observed on the root side

(a)

(b)

(c)

(d)
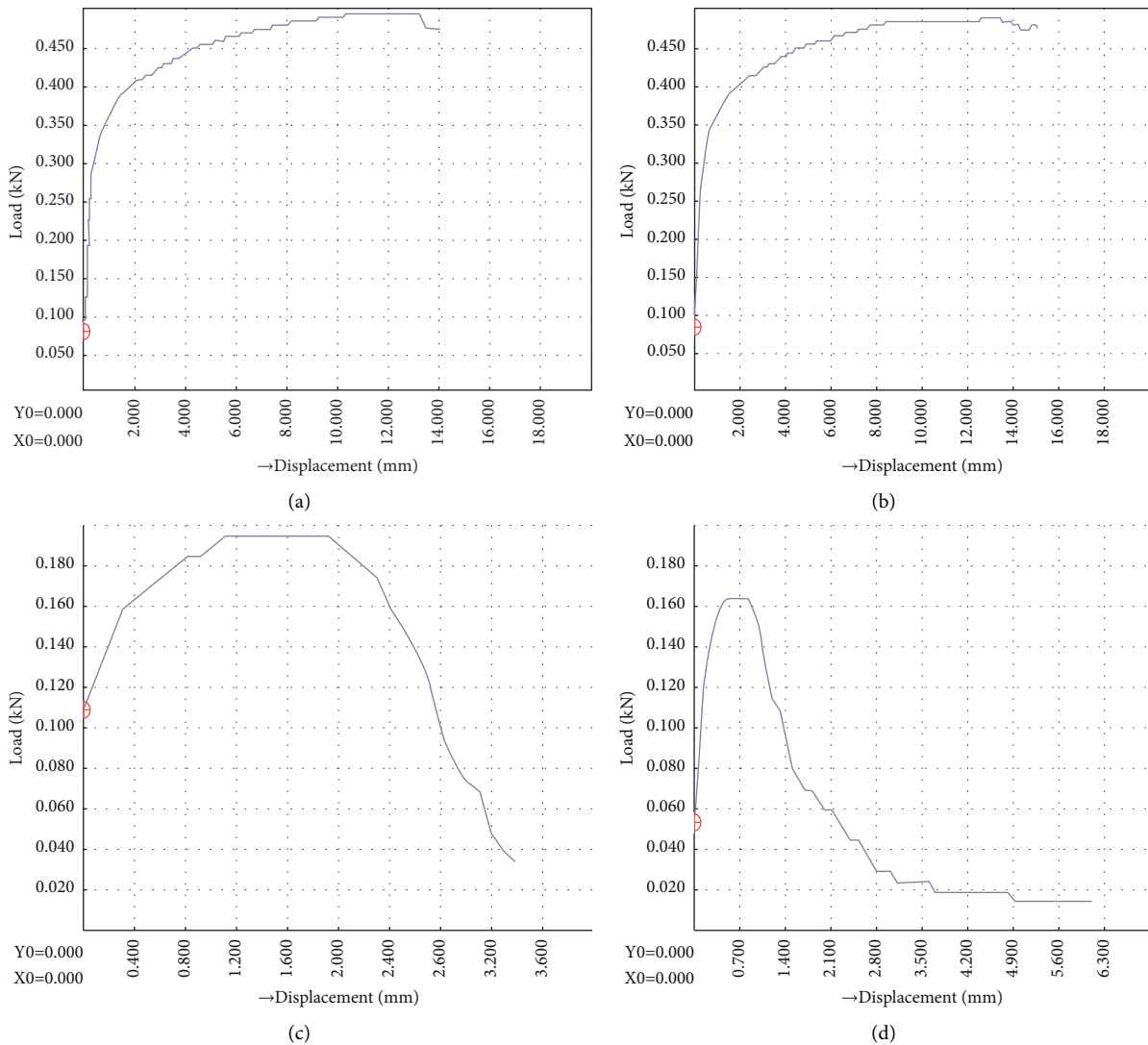
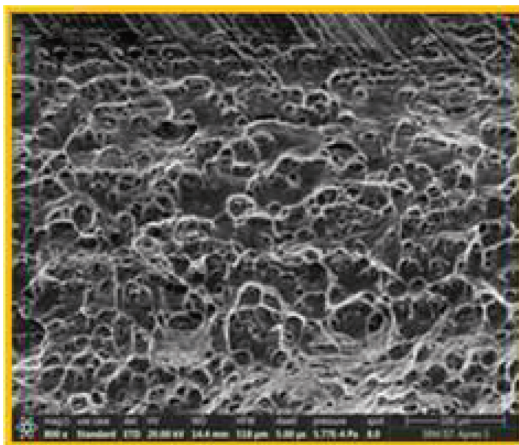FIGURE 8: Graphical representation of bending strength values.

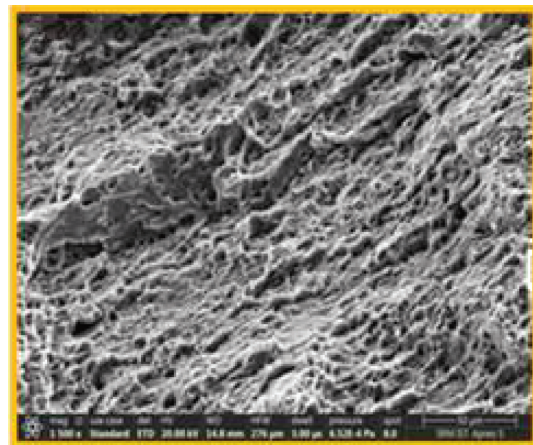Figure 9: Fractography of tensile test specimen.
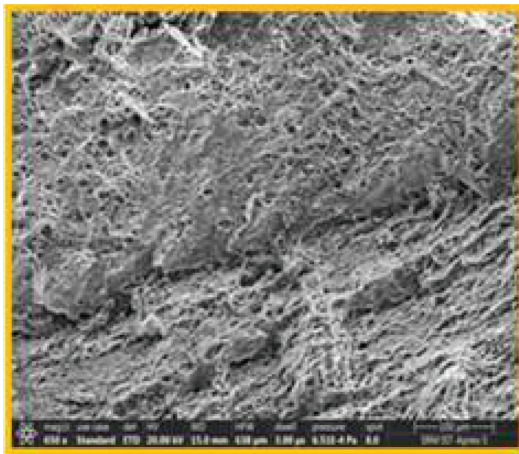
(a)
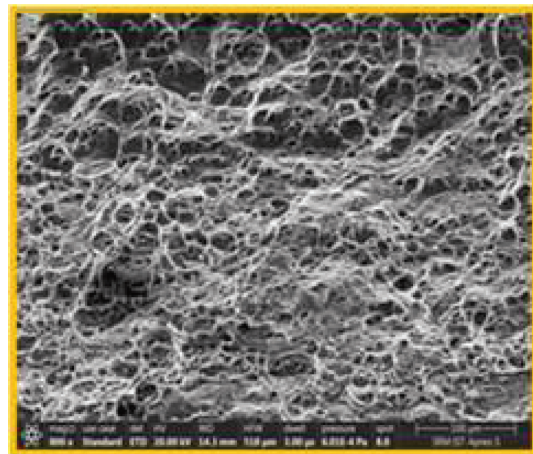
(b)

(c)

(d)

Figure 10: SEM images of tensile fractured weld samples.

5. Conclusions

FSW joints were successfully fabricated with the tapered pin tool for various process parameter combinations. In addition, the microhardness, tensile strength, yield strength, bending strength, and microstructural characteristics of AA6082-AA7075 dissimilar weld joints were studied, and the following conclusions were derived;

(i) The micro- and macrostructures of the dissimilar FSW joints are analyzed utilizing rotational tool speed, tool traverse speed, tool pin profile, and tool plunge speed.

(ii) The rotational and welding speed influences the weld joints' hardness and tensile strength value in the dissimilar joining of metals using FSW.

(iii) The highest hardness values of the weld specimens were achieved at the rotational tool speed of 2300 rpm, tool traveling rate of 40 mm/min, and tool plunge speed of 30 mm/min. On the other hand, the samples processed at the rotational speed of 1600 rpm, tool travel speed of 30 mm/min, and tool plunge speed of 20 mm/min exhibited the most negligible hardness. The maximum and minimum hardness values attained were 145 Hv and 102 Hv, respectively.

(iv) The high tensile strength of 191 MPa was achieved for the rotational tool speed of 2300 rpm, welding speed of 40 mm/min, and tool plunge speed of 30 mm/min. On the other hand, the low tensile strength of 125 MPa was obtained at a rotation tool speed of 1600 rpm and welding speed of 40 mm/min.

(v) Bending tests revealed that the maximum bending strength of 114.23 N/mm^2 was obtained at the ultimate breaking load of 0.495 kN, and the minimum bending strength of 25.38 N/mm^2 was obtained with an ultimate breaking load of 0.195 kN.

(vi) The results indicated that the tool rotation speed and tool travel speed significantly influence the microstructure and the behaviors of dissimilar AA6082-AA7075 weld joints. However, the tool plunge speed modified the properties due to its interaction with the other two parameters.

Data Availability

The data used to support the findings of this study are included in the article.

Conflicts of Interest

The authors declare that there are no conflicts of interest regarding the publication of this article.

References

[1] N. Z. Khan, A. N. Siddiquee, Z. A. Khan, and S. K. Shihab, "Investigations on tunneling and kissing bond defects in FSW joints for dissimilar aluminum alloys," *Journal of Alloys and Compounds*, vol. 648, pp. 360–367, 2015.

[2] P. Srinivasulu, G. Krishna Mohan Rao, and M. Satyanarayana Gupta, "Evaluation of bending strength of friction stir welded AA 6082 aluminum alloy butt joints," *International Journal of Advance Research in Science and Engineering*, vol. 4, no. 1, pp. 1262–1270, 2015.

[3] K. Giridharan and P. Sevvel, "Experimental Study on Mechanical Properties of Friction Stir Welded Dissimilar Joints of Aluminum Alloys AA8011-AA6082," *International Journal of Vehicle Structure and Systems*, vol. 11, no. 2, pp. 135–139, 2019.

[4] K. Giridharan, G. Chakravarthi, S. Karthick, S. MuthuKumaran, S. Padmanaban, and M. Kabeerr, *Investigation on Mechanical Properties of AA6082-AA7075 Friction Stir Welded Dissimilar Aluminum Alloys*, Springer, Berlin, Germany, 2021.

[5] M. K. Gupta, "Effects of tool profile on mechanical properties of aluminium alloy Al 1120 friction stir welds," *Journal of Adhesion Science and Technology*, vol. 34, no. 18, pp. 2000–2010, 2020.

[6] G. Karrar, A. Galloway, A. Toumpis, H. Li, and F. Al-Badour, "Microstructural characterisation and mechanical properties of dissimilar AA5083-copper joints produced by friction stir welding," *Journal of Materials Research and Technology*, vol. 9, no. 5, pp. 11968–11979, 2020.

[7] B. Stalin, M. Ravichandran, G.T. Sudha et al., "Effect of titanium diboride ceramic particles on mechanical and wear behaviour of Cu-10 wt% W alloy composites processed by P/M route," *Vacuum*, vol. 184, Article ID 109895, 2021.

[8] S. D. Kumar, M. Ravichandran, A. Jeevika, B. Stalin, C. Kailasanathan, and A. Karthick, "Effect of ZrB2 on microstructural, mechanical and corrosion behaviour of aluminium (AA7178) alloy matrix composite prepared by the stir casting route," *Ceramics International*, vol. 47, no. 9, pp. 12951–12962, 2021.

[9] K. Yoganandam, V. Shanmugam, A. Vasudevan et al., "Investigation of dynamic, mechanical, and thermal properties of calotropis procera particle-reinforced pla biocomposites," *Advances in Materials Science and Engineering*, vol. 2021, Article ID 2491489, 7 pages, 2021.

[10] H. Goodarzi Hosseinabadi and S. Serajzadeh, "Hot extrusion process modeling using a coupled upper bound- finite element method," *Journal of Manufacturing Processes*, vol. 16, 2014.

[11] P. Cavaliere and A. Squillace, "High temperature deformation of friction stir processed 7075 aluminium alloy," *Materials Characterization*, vol. 55, 2005.

[12] M. Sadeghi-Ghogheri, M. Kasiri-Asgarani, and K. Amini, "Friction stir welding of dissimilar joint of aluminum alloy 5083 and commercially pure titanium," *Metallic Materials*, vol. 54, 2016.

[13] T. Sathish, V. Mohanavel, A. Karthick, M. Arunkumar, M. Ravichandran, and S. Rajkumar, "Study on Compaction and machinability of silicon nitride (Si3N4) reinforced copper alloy composite through P/M route," *International Journal of Polymer Science*, vol. 2021, Article ID 7491679, 10 pages, 2021.

[14] B. Gungor, E. Kaluc, E. Taban, and A. Sik, "Mechanical, fatigue and microstructural properties of friction stir welded 5083-H111 and 6082-T651 aluminum alloys," *Materials & Design (1980-2015)*, vol. 56, pp. 84–90, 2014.

[15] K. A. Ali, V. Mohanavel, M. Ravichandran, S. A. Vendan, T. Sathish, and A. Karthick, "Microstructure and Mechanical

properties of friction stir welded SiC/TiB$_2$ reinforced aluminum hybrid composites," *Silicon*, pp. 1–11, 2021.

[16] E. Cetkin, Y. H. Çelik, and S. Temiz, "Microstructure and mechanical properties of AA7075/AA5182 jointed by FSW," *Journal of Materials Processing Technology*, vol. 268, pp. 107–116, 2019.

[17] K. N. Syed and M. D. Touseef, "Mechanical properties of friction stir welding joints of similar and dissimilar aluminum alloys AA6061 and AA6082," *International Journal of Mechanical Engineering and Technology*, vol. 7, no. 4, pp. 256–266, 2016.

[18] P. Sevvel, C. Satheesh, and V. Jaiganesh, "Influence of tool rotational speed on microstructural characteristics of dissimilar Mg alloys during friction stir welding," *Transactions of the Canadian Society for Mechanical Engineering*, vol. 43, no. 1, pp. 132–141, 2019.

[19] T. Sathish, S. Tharmalingam, V. Mohanavel et al., "Weldability investigation and optimization of process variables for TIG-welded aluminium alloy (AA 8006)," *Advances in Materials Science and Engineering*, vol. 2021, Article ID 2816338, 17 pages, 2021.

[20] S. Chinchanikar, S. Gharde, and M. Gadge, "Investigation of tool forces, weld bead micro-hardness and surface roughness during friction stir welding of aluminium 6063 alloy," *Advances in Materials and Processing Technologies*, 2020.

[21] C. B. Jagadeesha, "RETRACTED: Dissimilar friction stir welding between aluminum alloy and magnesium alloy at a low rotational speed," *Materials Science and Engineering: A*, vol. 616, pp. 55–62, 2014.

[22] R. Ashok Kumar and M. Rathinam Thansekhar, "Property evaluation of friction welded dissimilar metals:Aa6101-T6 and AA1350 Aluminum alloys," *Materials Science*, vol. 23, pp. 1392–1320, 2017.

[23] J. Li, Y. Shen, W. Hou, and Y. Qi, "Friction stir welding of Ti-6Al-4V alloy: Friction tool, microstructure, and mechanical properties," *Journal of Manufacturing Processes*, vol. 58, pp. 344–354, 2020.

[24] R. Palanivel, P. Koshy Mathews, N. Murugan, and I. Dinaharan, "Effect of tool rotational speed and pin profile on microstructure and tensile strength of dissimilar friction stir welded AA5083-H111 and AA6351-T6 Aluminum alloys," *Materials & Design*, vol. 40, pp. 7–16, 2012.

[25] U. das and V. Toppo, "Bending strength evaluation of friction stir welded AA6101-T6 and AA6351-T6 aluminum alloys butt joint," *Materials Today: Proceedings*, vol. 5, no. 5, pp. 11556–11562, 2018.

[26] V. Chitturi, S. R. Pedapati, and M. Awang, "Challenges in dissimilar friction stir welding of aluminum 5052 and 304 stainless steel alloys," *Materialwissenschaft und Werkstofftechnik*, vol. 51, no. 6, pp. 811–816, 2020.

[27] H. Deng, Y. Chen, Y. Jia et al., "Microstructure and mechanical properties of dissimilar NiTi/Ti6Al4V joints via back-heating assisted friction stir welding," *Journal of Manufacturing Processes*, vol. 64, pp. 379–391, 2021.

[28] S. Emami, S. Sadeghi-Kanani, T. Saeid, and F. Khan, "Dissimilar friction stir welding of AISI 430 ferritic and AISI 304L austenitic stainless steels," *Archives of Civil and Mechanical Engineering*, vol. 20, no. 131, 2020.

[29] D. P. Pushpanath, K. G. Balamuruga, and K. Mahadevan, "Investigation on the change effected by the tool type on the hardness of friction stir processed AA6063 aluminium alloy," *Journal of Applied Sciences*, vol. 12, no. 10, pp. 1067–1070, 2012.

[30] S. Balamurugan, K. Jayakumar, and K. Subbaiah, "Influence of friction stir welding parameters on dissimilar joints AA6061-T6 and AA5052-H32," *Arabian Journal for Science and Engineering*, 2021.

[31] A. Eyvazian, A. Hamouda, F. Tarlochan, H. A. Derazkola, and F. Khodabakhshi, "Simulation and experimental study of underwater dissimilar friction-stir welding between aluminium and steel," *Journal of Materials Research and Technology*, vol. 9, no. 3, pp. 3767–3781, 2020.

[32] H. A. Derazkola, E. García, A. Eyvazian, and M. Aberoumand, "Effects of rapid cooling on properties of aluminum-steel friction stir welded joint," *Materials*, vol. 14, no. 4, 2021.

[33] Y. Guo, Y. Ma, X. Zhang, X. Qian, and J. Li, "Study on residual stress distribution of 2024-T3 and 7075-T6 aluminum dissimilar friction stir welded joints," *Engineering Failure Analysis*, vol. 118, Article ID 104911, 2020.